# High-Performance Alkaline Water Electrolysis: A Membrane– Catalyst–Device Integrated Paradigm

Shubham Mishra[1,2#], Sarthak Mishra [1,2#], Vartika Sharma[1,2], Debashish Sarkar[3], Vaibhav Kulshrestha [1, 2 *]

[1] Council of Scientific and Industrial Research- Central Salt and Marine Chemical Research Institute, Bhavnagar, Gujarat, India-364002

[2] Academy of Scientific and Innovative Research (AcSIR), Ghaziabad, Uttar Pradesh, India-201002

[3] Department of Physics, Malviya National Institute of Technology, Jaipur, India

*** Email:** *vaibhavphy@gmail.com; vaibhavk@csmcri.res.in*

## Table of Contents

- S-2. High-resolution XPS spectra of PhosTriOx.
- S-3. FTIR spectrum of the interpolymer film.
- S-4. SEM-EDX mapping and compositional analysis of PhosTriO7.
- S-5. TEM and HRTEM analysis of PhosTriO7 heterostructure.
- S-6. AFM surface topography of Styrion AEM.
- S-7. Thermogravimetric analysis (TGA/DTG) of Styrion AEM.
- S-8. Mechanical stress–strain analysis of Styrion AEM.
- S-9. HER polarization curves and Tafel analysis of PhosTriOx catalysts.
- S-10. EIS Nyquist plots of PhosTriOx under HER conditions.
- S-11. Electrochemical kinetic analysis (Cdl, ECSA, TOF) for HER.
- S-12. OER polarization curves and Tafel analysis of PhosTriOx catalysts.
- S-13. EIS Nyquist plots of PhosTriOx under OER conditions.
- S-14. Electrochemical kinetic analysis (Cdl, ECSA, TOF) for OER.
- S-15. Chronoamperometric stability of PhosTriO7 for HER.
- S-16. Chronoamperometric stability of PhosTriO7 for OER.
- S-17. ECSA normalized overpotential for HER & OER at 10 mA $cm^{-2}$ in 1.0 M KOH
- S-18: Post mortem FE-SEM and TEM analyses of Phos TriO7 catalyst
- Table S1: Atomic % of the different elements presented in the catalyst
- Table S2: Physicochemical properties of the Styrion AEM after 250hr stability test where: IEC (ion exchange capacity ($meqg^{-1}$), IC (Ionic conductivity, $mScm^{-1}$) and WU (water uptake(%)

## SI-1. Physiochemical characterization

### 1.1. Water uptake (WU) and ion-exchange capacity (IEC)

To determine the water uptake (WU), a 2.0 x 2.0 cm² membrane sample was vacuum dried for 24 hours and subsequently weighed in its dry state. The dry membrane was then immersed in distilled water for 24 hours to achieve maximum water absorption. Water uptake was calculated using the following equation: [1,2,3,4]:

$$WU\ (\%) = \frac{\Delta W}{W_{Dry}} x\ 100; \Delta W = W_{Wet} - W_{Dry}$$

Here, the mass of the membrane piece in a wet and dry state is abbreviated as $W_{Wet}$ & $W_{Dry}\ respectively$.

Water uptake (WU) and ion exchange capacity (IEC) are complementary parameters that are proportionally dependent on each other. IEC quantifies the extent of exchangeable ionic sites (expressed in milliequivalents) per unit dry membrane mass, which is related to the density of sulfonic acid groups (-$SO_3H$) within the membrane. A higher PEC generally indicates a greater density of -$SO_3H$ groups. The IEC Styrion membrane samples was determined using a simple neutralization titration method at 28 ± 2°C. Membrane samples (2.0 x 2.0 cm²) were soaked in 50 mL of 0.1 N HCl for 24 hours to convert all ionic sites to their $H^+$ form. Subsequently, the membranes were immersed in 50 mL of 0.1 N NaCl solution for an additional 24 hours to exchange $Na^+$ ions with $H^+$ ions in the membranes. The amount of $H^+$ released was quantified by titrimetric analysis using 0.1 M NaOH with phenolphthalein as the indicator. IEC was calculated using the following equation: [1,2,3,4]:

$$IEC = \frac{V \times C_{NaOH}}{W_{Dry}}$$

where V, $C_{NaOH}$ and $W_{Dry}$ are the titrant volume, concentration of NaOH solution (0.1M) and dry weight of membrane sample respectively

A remarkable balance between WU and PEC is crucial not only for maintaining membrane stability but also for enhancing performance in applications. This balance facilitates ionic mobility through the membrane while providing adequate abrasion resistance.

### 1.2. Ionic Conductivity

The ionic conductivity of the prepared membranes was measured using AC impedance spectroscopy. The membranes were pre-equilibrated in a 0.1 M NaCl solution for 24 hours. Styrion membranes were then placed within an in-house manufactured acrylic assembly equipped with stainless-steel circular electrodes of 1.0 $cm^2$ area. These electrodes were immersed in a 0.1 M NaCl solution, serving, as the conducting medium. An AC signal was applied to the electrodes, and the impedance was recorded over a frequency range of $10^6$ to 1 Hz at a scan rate of $10^{-6}$ A $s^{-1}$, generating a Nyquist plot. The resulting data were fitted to an appropriate model to determine the membrane resistance. The conductivity of the membrane was calculated using the following formula[1,2,3,4]:

$$Km\left(S\ cm^{-1}\right) = \frac{L\ (cm)}{R\ (\Omega) x\ A\left(cm^2\right)}$$

Here, L is membrane thickness corresponds to distance between the electrodes, R is the resistance obtained, and A is the effective area of the SS-electrode.

## SI-2 Detailed procedure for sample preparation and configurations of instruments employed for analysis

**SI-2.1.** Topographic imaging and composite dispersibility in the membrane were evaluated through semi-contact mode (SC mode) using an Ntegra Aura AFM instrument, AFM probe with micro fabricated cantilever operated at ambient temperature and open-air environment at 50 scans per minute over an effective area of 4 $\mu m^2$. Before characterization, the membrane film was kept at 60°C in vacuum oven for 48h.

**SI-2.2.** Field-emission scanning electron microscopy (FE-SEM) was used to probe the surface and cross-sectional morphology of Styrion membranes. The sample were prepared by parallelly rupturing the membranes in liquid $N_2$. Before analysis, Au-sputtering was performed to induce electrical conduction. Surface and cross-section images show that these membranes are dense in nature and no internal porous channel are formed.

**SI-2.3.** The tensile properties and stress-strain curve was evaluated from the results obtained using universal testing machine (UTM) Zwick Roell BT-FR2.5$^{TH}$.40 at 25 ± 2°C and at a stable crosshead speed of 2.0 mm per minute. Sample was prepared by cutting the membranes in long

strips of dimension length x breadth (5.0 cm x 0.5 cm) and transitioned between the clutches of UTM device, the force/stress inhomogeneity was maintained by modulating the dimensions carefully.

**SI-3 Electrochemical Evaluation of Catalytic Activity and Kinetic Parameters**

Electrochemical characterizations of the synthesized electrocatalysts were conducted using an Autolab M204 PGSTAT potentiostat/galvanostat system equipped with a three-electrode configuration. An Ag/AgCl electrode functioned as the reference electrode, while a glassy carbon electrode (GCE) with a 3 mm diameter served as the working electrode, and a graphite rod was employed as the counter electrode. Linear sweep voltammetry (LSV) measurements were acquired following the stabilization of the electrochemical signals by performing multiple potential sweeps in 1 M KOH for the Hydrogen evolution reaction (HER) and oxygen evolution reaction (OER). The potential windows were set from 0 to −1.0 V (vs. Ag/AgCl) for HER and 0 to 1.0 V for OER, with a scan rate of 5 mV $s^{-1}$. To ensure accurate potential referencing, the measured potentials were calibrated to the reversible hydrogen electrode (RHE) scale using the Nernst equation, thereby enabling standardized comparison of electrocatalytic performance across different systems.

$$E_{RHE} = E_{(Ag/AgCl)} + E^0\left(\frac{Ag}{AgCl}\right) + 0.059 \times pH \qquad (1)$$

Where $E_{(Ag/AgCl)}$ represents the empirically determined potential versus the Ag/AgCl reference electrode obtained during electrochemical measurements, and $E^0\left(\frac{Ag}{AgCl}\right)$ denotes the standard electrode potential of Ag/AgCl, which is 0.197 V. The term $E_{RHE}$ corresponds to the reversible hydrogen electrode (RHE) potential, which is adjusted according to the pH of the electrolyte medium, being 14 for 1 M KOH solution (alkaline condition). The conversion from the Ag/AgCl scale to the RHE scale ensures accurate thermodynamic referencing of the applied potentials.

From the LSV curve for OER process, overpotential of catalyst was calculated by following equation:

$$\eta = E_{RHE} - 1.23V \qquad (2)$$

The catalysts electrochemical kinetics were examined using Tafel equation, which is

$$\eta = a + b\log|j| \qquad (3)$$

where, $|j|$ is the observed current density, " $a$ " is a constant factor, "$b$" is the Tafel slope, and " $\eta$ " is the overpotential in this equation. The double-layer capacitance ($C_{dl}$) was calculated in order to calculate the electrochemical active surface area (ECSA) of the catalyst. Using CV, ECSA was computed at multiple scan rates (20–200 mV $s^{-1}$) to maximize $C_{dl}$ in non-faradaic realm. A frequency window of 100 kHz to 10 Hz, an AC amplitude of 10 mV was used for electrochemical impedance spectroscopy (EIS). Further, the stability of the test sample for HER as well as OER was assessed by employing a chronoamperometric test at the obtained overpotential values.

**SI-3.1 Turn Over Frequency (TOF)**

Turnover Frequency (TOF) is a key kinetic parameter used to evaluate the intrinsic activity of electrocatalysts in water splitting. It is defined as the number of product molecules (such as $H_2$ or $O_2$) generated per active catalytic site per unit time, thereby reflecting the efficiency of each individual site rather than the overall catalyst loading or surface area. Unlike current density or overpotential, which are influenced by electrode geometry, catalyst mass, and morphology, TOF provides a true measure of the catalytic performance that can be directly compared across different materials. In electrolytic water splitting, determining TOF is essential because it allows researchers to distinguish whether improved performance arises from an increase in the number of active sites or from higher intrinsic activity of those sites. This insight is critical for rational catalyst design, enabling the development of materials with both high site density and superior per-site activity, which together are necessary for achieving efficient and scalable hydrogen and oxygen production.

$$TOF = \frac{j \times A}{z \times F \times n}$$

Where, j= Current densit, A= surface area of working electrode, z= no. of electrons transfer (for HER=2 & OER=4), F = Faraday constant (96485 A s $mol^{-1}$) and n = no. of moles of active sites

**SI-3.2 Electrochemically Active Surface Area (ECSA):**

Electrochemically Active Surface Area (ECSA) is a parameter that quantifies the real surface area of a catalyst that actively participates in electrochemical reactions, such as the hydrogen evolution reaction (HER) and oxygen evolution reaction (OER) in water splitting. Unlike the geometric electrode area, ECSA reflects the true number of accessible active sites exposed to the electrolyte

during catalysis. A higher ECSA generally indicates that more catalytic sites are available, leading to higher current densities for a given overpotential.

The most common experimental method is based on the double-layer capacitance ($C_{dl}$) measurement: Select a non-faradaic potential window (where no redox processes occur), Record cyclic voltammetry (CV) curves at different scan rates (e.g., 20–200 mV/s), Plot the capacitive current density ($\Delta j = (ja - jc)/2$) at a fixed potential against the scan rate, The slope of this linear plot gives the double-layer capacitance ($C_{dl}$), ECSA is then estimated using:

$$ECSA = \frac{Cdl}{Cs}$$

where Cs is the specific capacitance of a smooth surface of the same material in the same electrolyte (typically 20–60 μF $cm^{-2}$, depending on the system).

**SI-3.2 Tafe Slope calculations:**

The Tafel slope is an electrochemical kinetic parameter that describes how the overpotential (η) required for a reaction change with current density (j). In electrocatalytic water splitting (HER and OER), it provides direct insight into the reaction mechanism and the rate-determining step. A smaller Tafel slope indicates that the reaction rate increases significantly with only a small increase in overpotential, reflecting superior catalytic kinetics. Typical values for HER are ~120, ~40, and ~30 mV $dec^{-1}$, which correspond to different rate-limiting steps (Volmer, Heyrovsky, or Tafel step, respectively), while OER mechanisms usually show slopes around 60–120 mV $dec^{-1}$.

The Tafel Slope is calculated by using the equation:

$$\eta = a + b\,log(j)$$

Where: η = overpotential (V), j = current density (mA $cm^{-2}$), a = intercept (related to exchange current density), b = Tafel slope (mV $dec^{-1}$). The slope of this line ($\Delta\eta/\Delta\log j$) gives the Tafel slope in units of mV $dec^{-1}$.

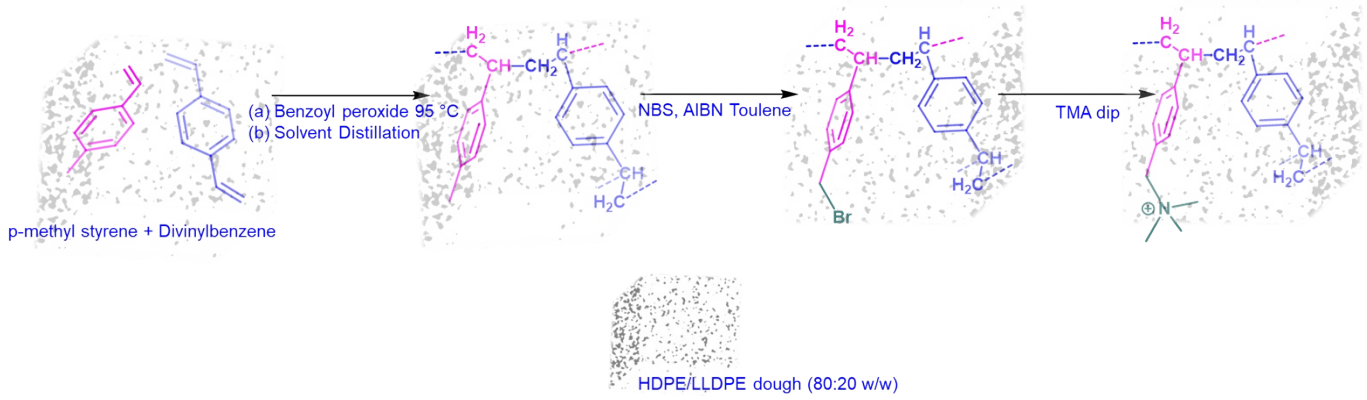


**S-1.** Schematic illustration of the synthesis pathway for the Styrion anion exchange membrane (AEM). The process involves radical copolymerization of *p*-methylstyrene and divinylbenzene in the presence of a HDPE/LLDPE (80:20 w/w) interpolymer matrix using benzoyl peroxide as the initiator. Subsequent solvent distillation yields the interpolymer framework, which undergoes benzylic bromination via NBS/AIBN in toluene, followed by quaternization with trimethylamine (TMA) to introduce β-elimination-resistant quaternary ammonium functionalities. This stepwise process produces a robust crosslinked AEM with tailored ionic domains for enhanced alkaline stability and conductivity.

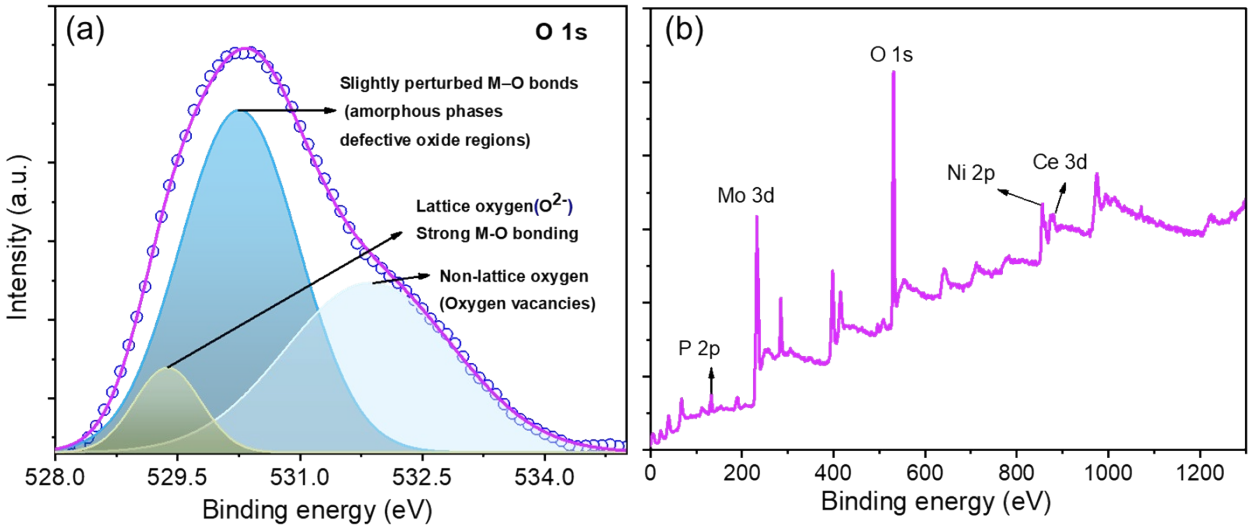


**S-2.** (a) High-resolution XPS O 1s spectrum of the PhosTriOx catalyst, deconvoluted into lattice oxygen (~529.4 eV), oxygen vacancies/defective oxygen sites (~531.0 eV), and adsorbed oxygen

species (~532.2 eV), confirming the presence of vacancy-rich domains favourable for catalytic activity. (b) Full XPS spectra of PhosTriOx .

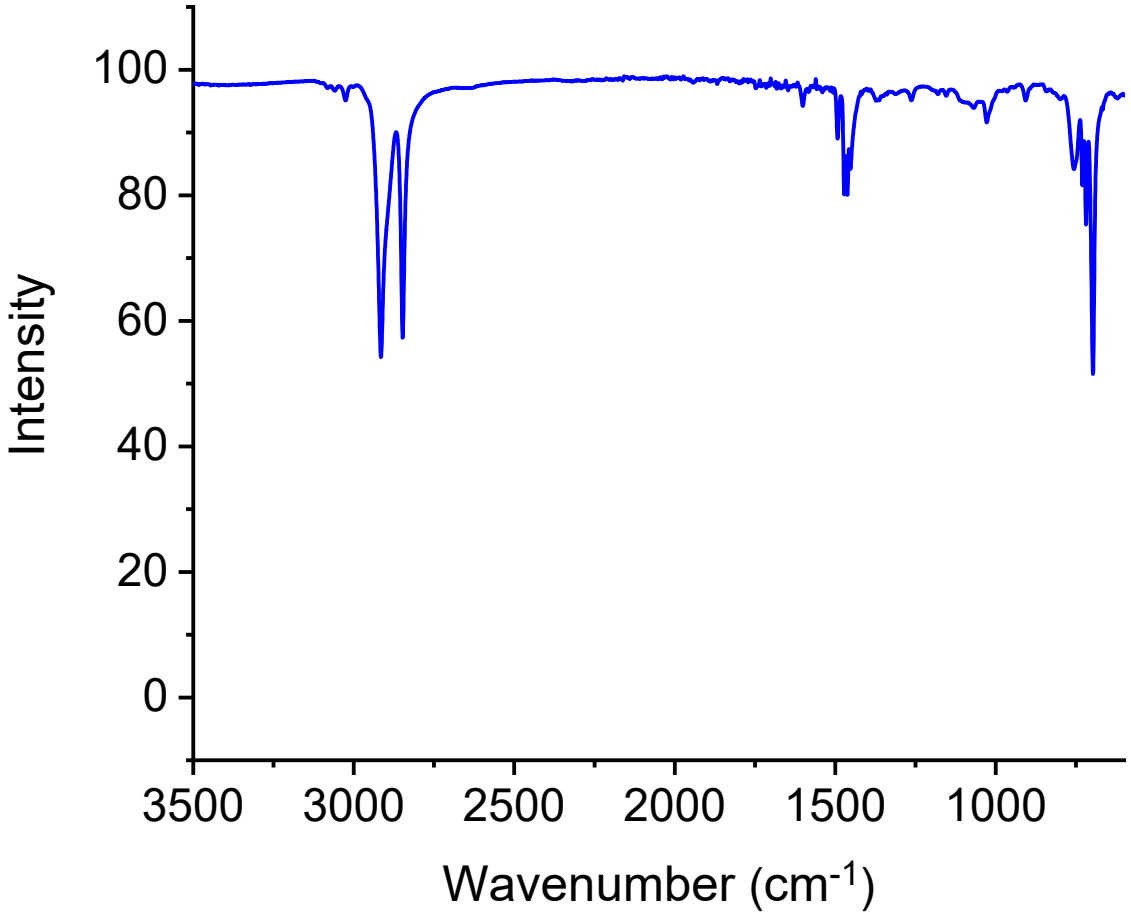


**S-3**: FTIR spectrum of the interpolymer film, confirming the successful incorporation of *p*-methylstyrene and divinylbenzene segments into the polyethylene backbone. The characteristic absorption bands include –$CH_2$– stretching vibrations at 2912 and 2850 $cm^{-1}$, aromatic C–H stretching at 3030 $cm^{-1}$, and C=C stretching at 1450 $cm^{-1}$, which collectively validate the structural integrity of the synthesized interpolymer matrix.

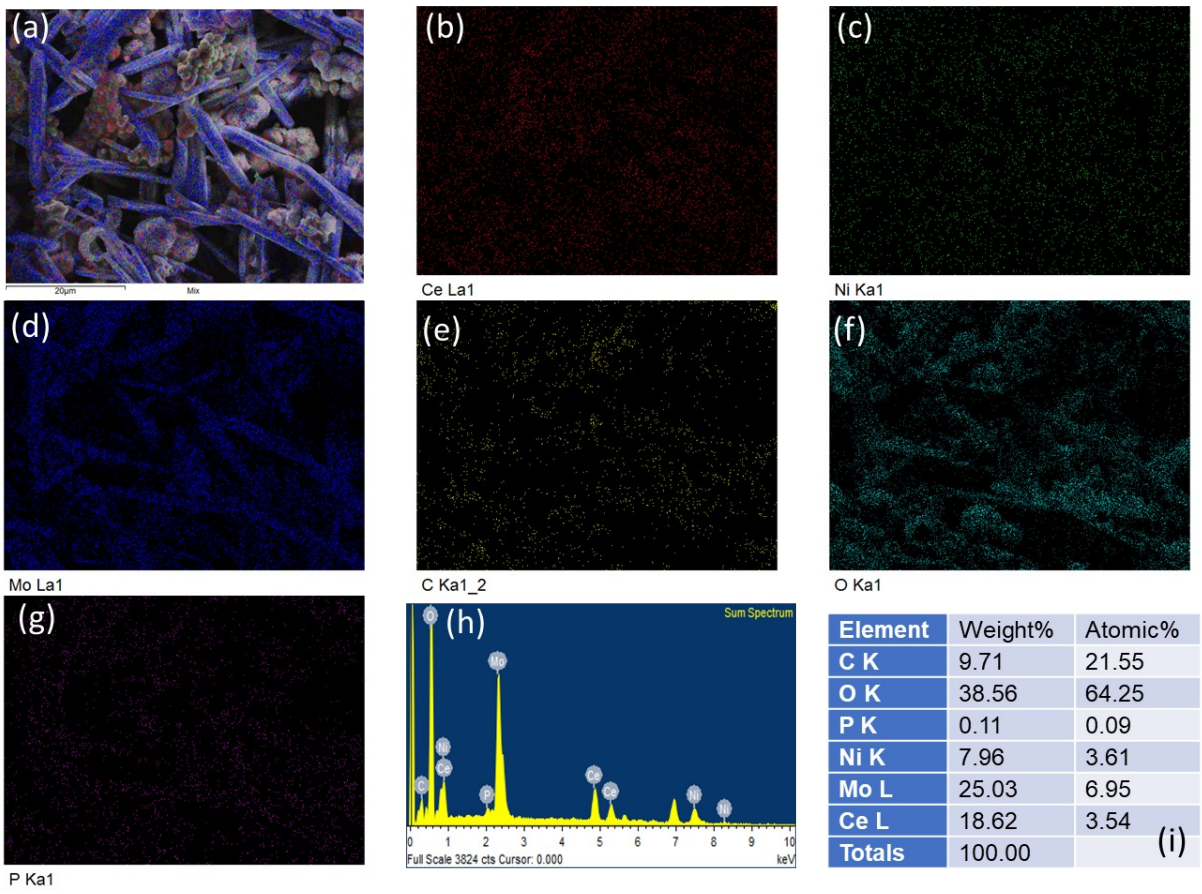


| Element | Weight% | Atomic% |
|---|---|---|
| C K | 9.71 | 21.55 |
| O K | 38.56 | 64.25 |
| P K | 0.11 | 0.09 |
| Ni K | 7.96 | 3.61 |
| Mo L | 25.03 | 6.95 |
| Ce L | 18.62 | 3.54 |
| Totals | 100.00 | |

(i)

**S-4:** SEM-EDX elemental mapping and compositional analysis of the PhosTriO7 catalyst. (a) SEM image of the catalyst morphology. Elemental distribution maps confirm homogeneous dispersion of (b) Ce, (c) Ni, (d) Mo, (e) C, (f) O, and (g) P throughout the heterostructure. (h) EDX spectrum showing the characteristic peaks of Ni, Mo, Ce, O, C, and P. (i) Quantitative EDS analysis table, indicating the elemental composition with major contributions from O (38.56 wt%), Mo (25.03 wt%), Ce (18.62 wt%), Ni (7.96 wt%), and C (9.71 wt%), alongside incorporation of P (0.11 wt%), confirming successful phosphorus doping into the Ni–Mo–Ce oxide framework.

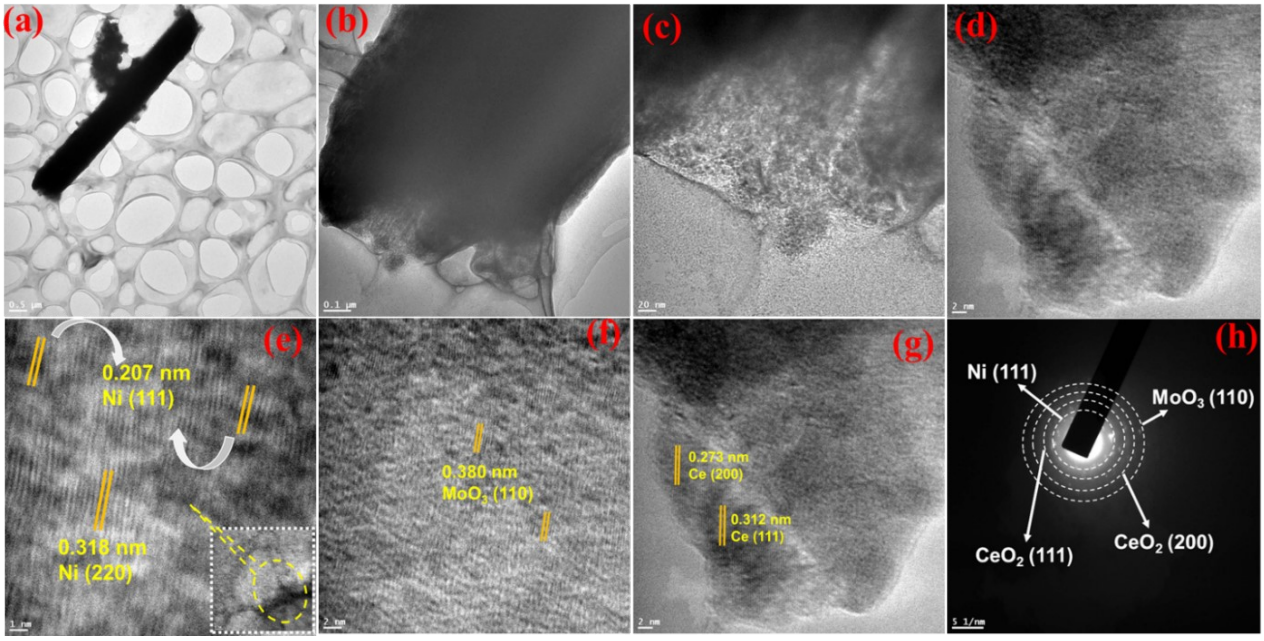


**S-5.** TEM and HRTEM analysis of the PhosTriO7 heterostructure. (a–b) Low-magnification TEM images showing rod-like morphology with uniform contrast. (c–d) High-resolution TEM (HRTEM) images revealing crystalline domains and heterointerfaces. (e) Lattice fringes indexed to Ni (111, 0.207 nm) and Ni (220, 0.318 nm), confirming the metallic Ni phase. (f) Lattice spacing of 0.380 nm corresponding to $MoO_3$ (110). (g) Lattice fringes of $CeO_2$ assigned to (200, 0.272 nm) and (111, 0.312 nm) planes, verifying the coexistence of $CeO_2$. (h) Selected area electron diffraction (SAED) pattern confirming polycrystalline nature and multiphase structure with reflections indexed to Ni, $MoO_3$, and $CeO_2$.

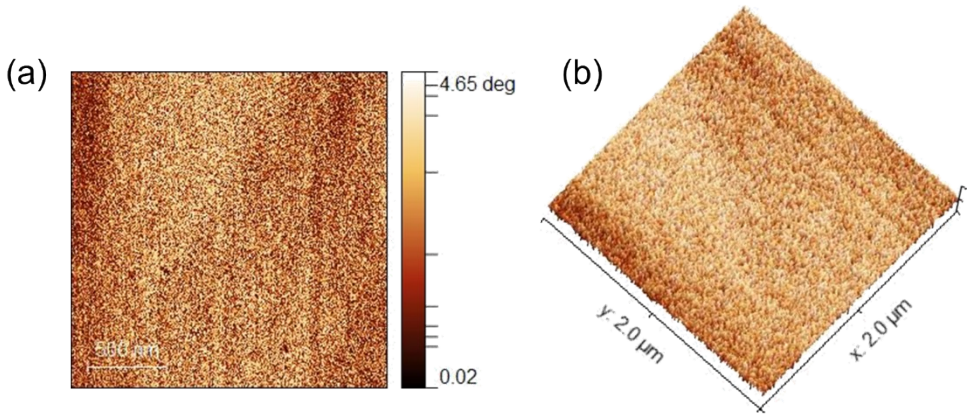


**S-6:**Atomic force microscopy (AFM) images of the Styrion anion exchange membrane surface: (left) 2D topographic view showing uniform morphology with minimal defects and well-

distributed ionic domains; (right) 3D height profile confirming smooth surface characteristics and interconnected nanophase domains conducive to efficient ion transport.

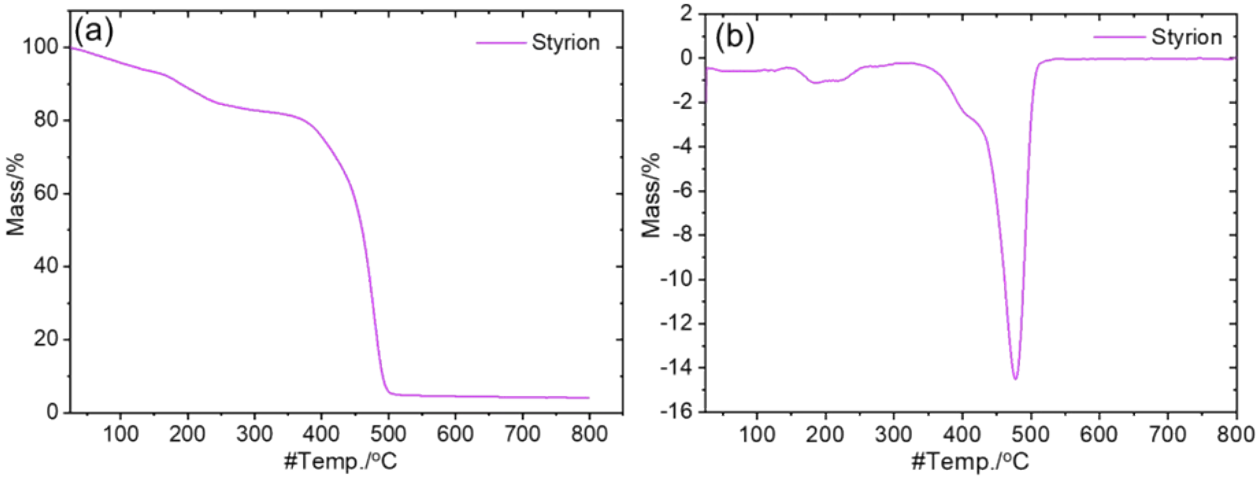


**S-7:** Thermogravimetric analysis (TGA) and derivative thermogravimetry (DTG) curves of the Styrion anion exchange membrane under a nitrogen atmosphere. The TGA profile (left) exhibits a three-step weight loss corresponding to (i) removal of adsorbed/bound water (~100–120 °C), (ii) degradation of functionalized cationic groups (200–400 °C), and (iii) decomposition of the polymer backbone (>400 °C). The DTG curve (right) highlights distinct degradation peaks, with the major decomposition occurring near ~475 °C, confirming the excellent thermal stability of the membrane.

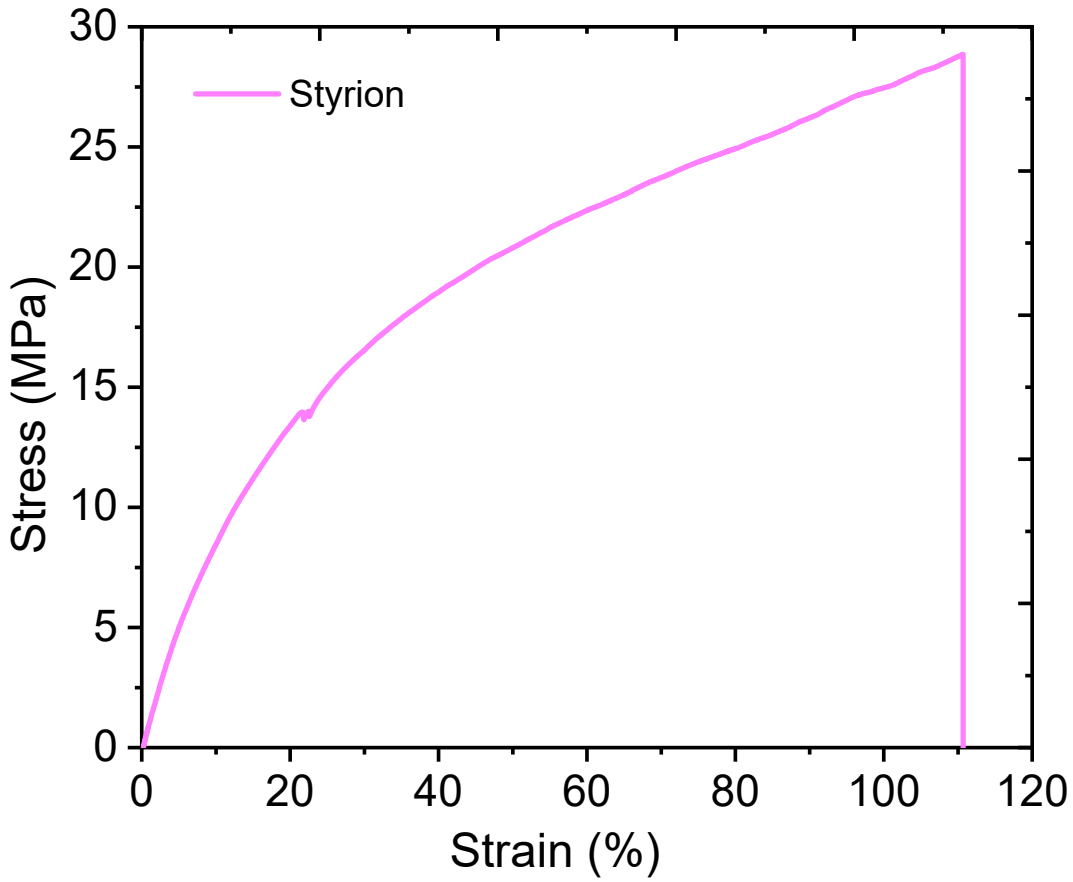


**S-8:** Mechanical characterisation of the Styrion anion exchange membrane. The stress–strain curve reveals excellent flexibility and mechanical robustness, with a Young's modulus of ~136 MPa and elongation at break of ~111%, indicating strong tensile strength and high strain tolerance. These properties confirm the membrane's suitability for durable operation in electrochemical water splitting under alkaline conditions.

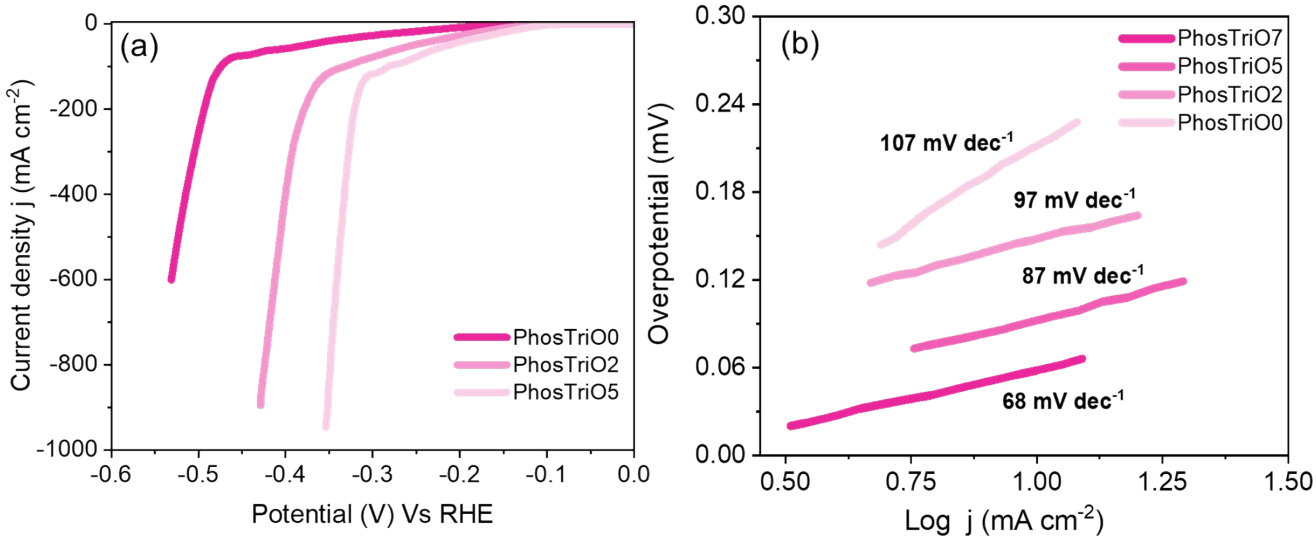


**S-9:**Electrochemical performance of phosphorus-doped PhosTriOx catalysts toward the hydrogen evolution reaction (HER) in 1.0 M KOH. (a) Linear sweep voltammetry (LSV) polarization curves showing progressive enhancement in HER activity with increasing phosphorus incorporation, with PhosTriO7 requiring the lowest overpotential compared to PhosTriO5, PhosTriO2, and undoped PhosTriO0. (b) Corresponding Tafel plots, where PhosTriO7 exhibits the smallest slope, indicating accelerated Volmer–Heyrovsky kinetics and more favorable hydrogen desorption dynamics.

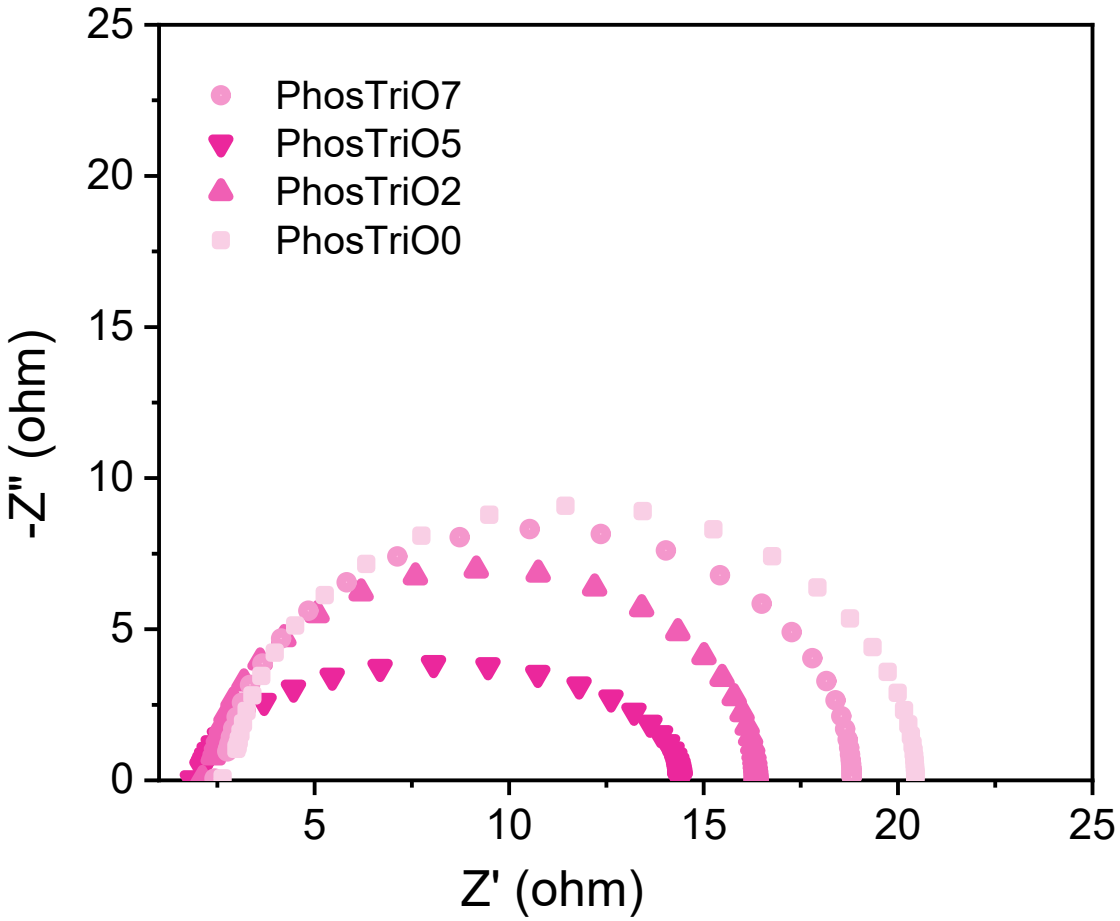


**S-10:** Electrochemical impedance spectroscopy (EIS) Nyquist plots of NMC-P-7, NMC-P-5, NMC-P-2, and NMC-P-0 catalysts recorded in 1.0 M KOH. Among all compositions, NMC-P-7 exhibits the smallest semicircle diameter, corresponding to the lowest charge-transfer resistance (Rct), indicative of superior interfacial charge transport and faster reaction kinetics compared to lower phosphorus-doped and undoped counterparts.

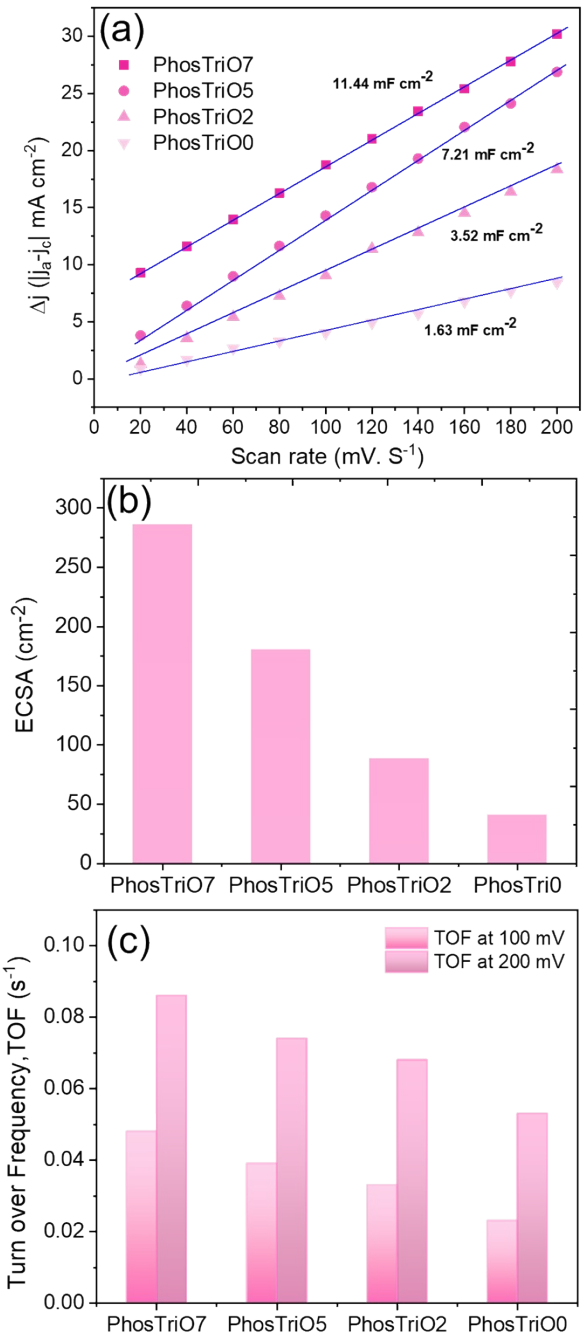


**S-11:** Electrochemical kinetic analysis of phosphorus-doped PhosTriOx catalysts for HER in 1.0 M KOH. (a) Comparison of double-layer capacitance (Cdl) values, revealing the highest Cdl for PhosTriO7, indicative of maximized electrochemically active surface area (ECSA). (b) ECSA plots confirming enhanced active site availability with increasing phosphorus incorporation. (c) Turnover frequency (TOF) values at 100 and 200 mV overpotential, demonstrating the superior intrinsic activity of PhosTriO7 relative to other compositions.

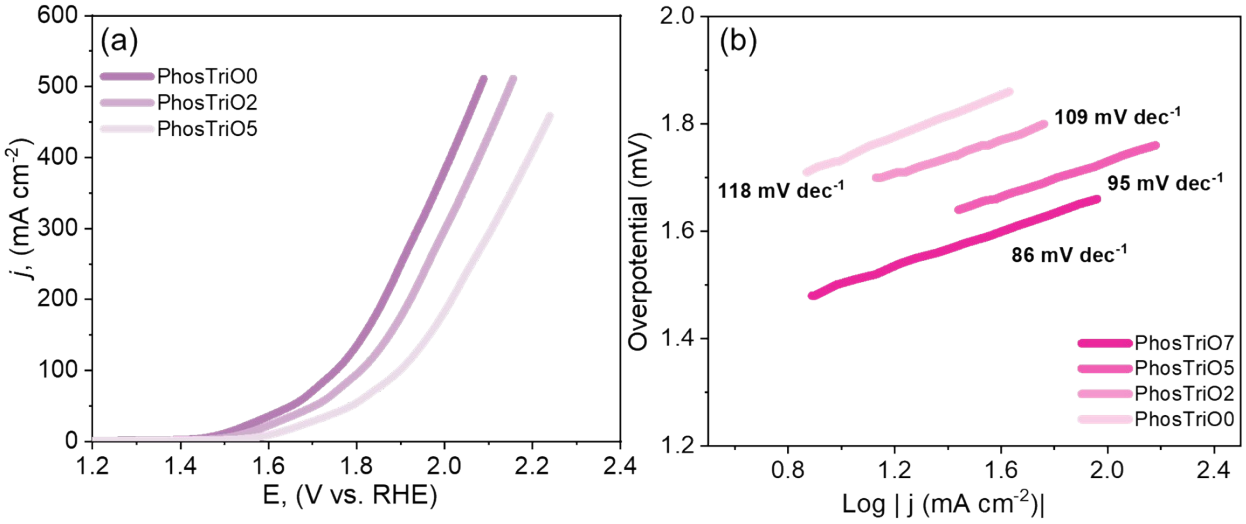


**S-12:** Electrocatalytic oxygen evolution reaction (OER) performance of PhosTriOx catalysts in 1.0 M KOH. (a) Linear sweep voltammetry (LSV) polarization curves of PhosTriO0, PhosTriO2, PhosTriO5 showing a systematic reduction in overpotential with increasing phosphorus incorporation. (b) Corresponding Tafel plots, highlighting improved reaction kinetics for phosphorus-doped catalysts, with PhosTriO7 exhibiting the smallest Tafel slope, indicative of accelerated charge-transfer dynamics and optimized OER pathways.

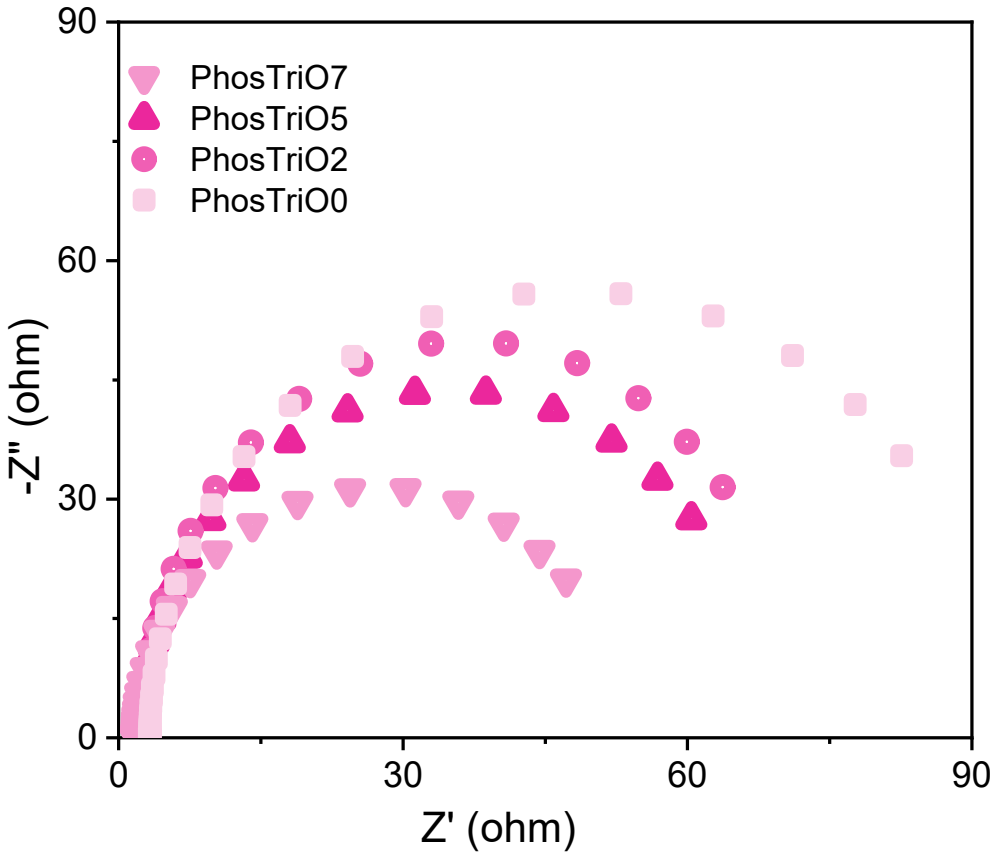


**S-13:** Electrochemical impedance spectroscopy (EIS) Nyquist plots of PhosTriOx catalysts (PhosTriO0, PhosTriO2, PhosTriO5, and PhosTriO7) recorded in 1.0 M KOH under OER-relevant conditions. The progressive decrease in charge-transfer resistance (Rct) with increasing phosphorus incorporation highlights the superior interfacial charge transport properties of PhosTriO7, consistent with its enhanced catalytic kinetics and improved electronic conductivity.

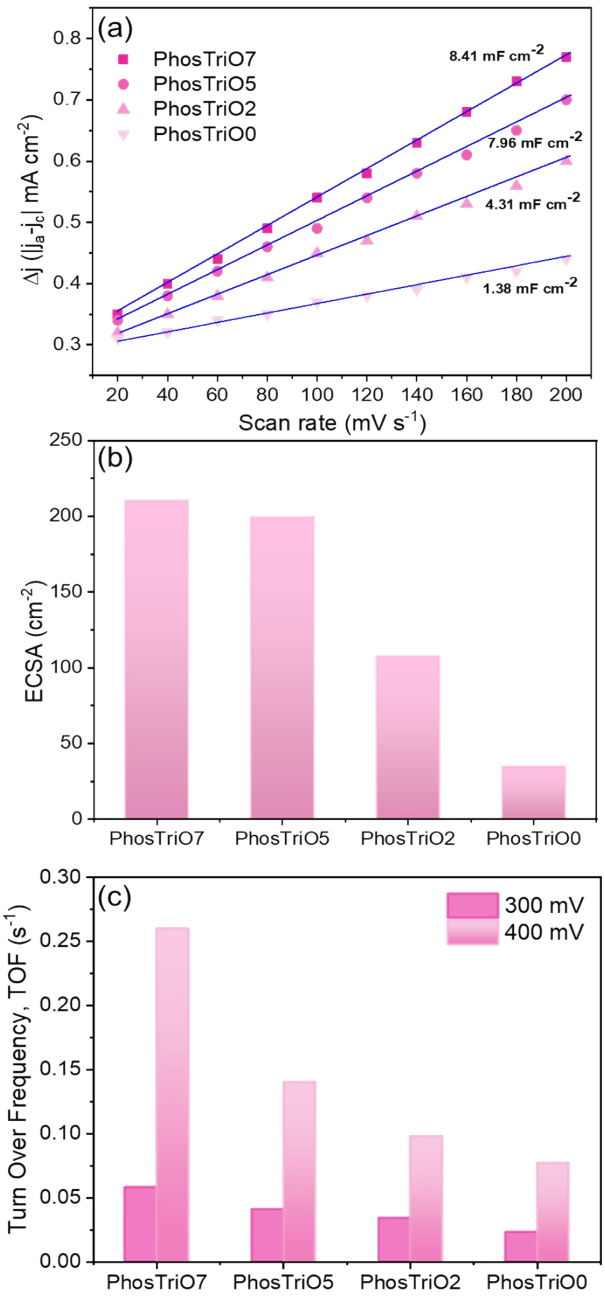


**S-14:** Electrochemical kinetic analysis of phosphorus-doped PhosTriOx catalysts in 1.0 M KOH. (a) Double-layer capacitance (Cdl) values obtained from cyclic voltammetry at different scan rates, used to estimate the electrochemically active surface area (ECSA). (b) ECSA plots highlighting the progressive increase in active surface sites with higher phosphorus incorporation, with PhosTriO7 exhibiting the maximum ECSA. (c) Comparison of turnover frequency (TOF) values at 100 mV, demonstrating the superior intrinsic HER activity of PhosTriO7. (d) TOF values at 200 mV, further confirming the enhanced catalytic efficiency of PhosTriO7 relative to PhosTriO5, PhosTriO2, and undoped PhosTriO0.

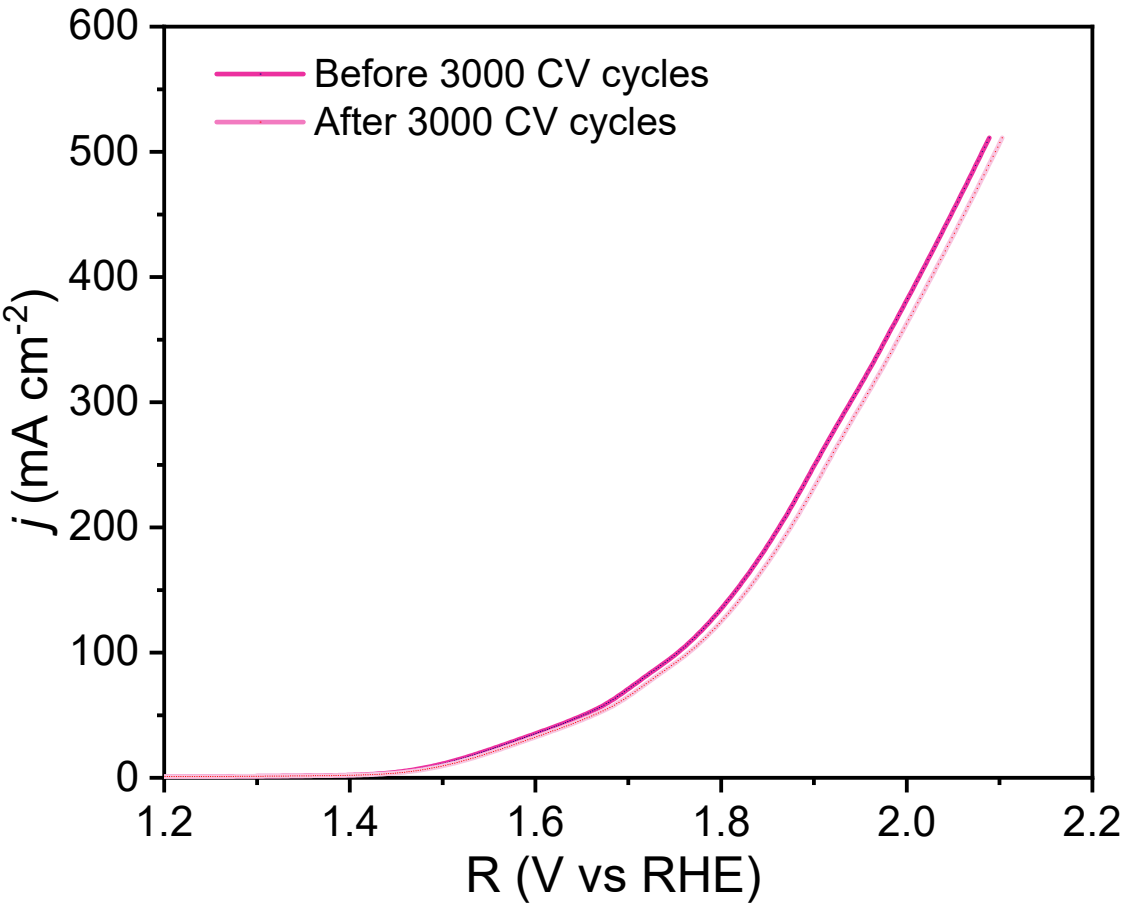


**S-15:** Chronoamperometric durability analysis of the PhosTriO7 catalyst for the hydrogen evolution reaction (HER) in 1.0 M KOH. The polarization curves recorded before and after 100 h of continuous operation exhibit negligible shifts, confirming the excellent electrochemical stability and sustained catalytic activity of PhosTriO7 under prolonged alkaline HER conditions**.**

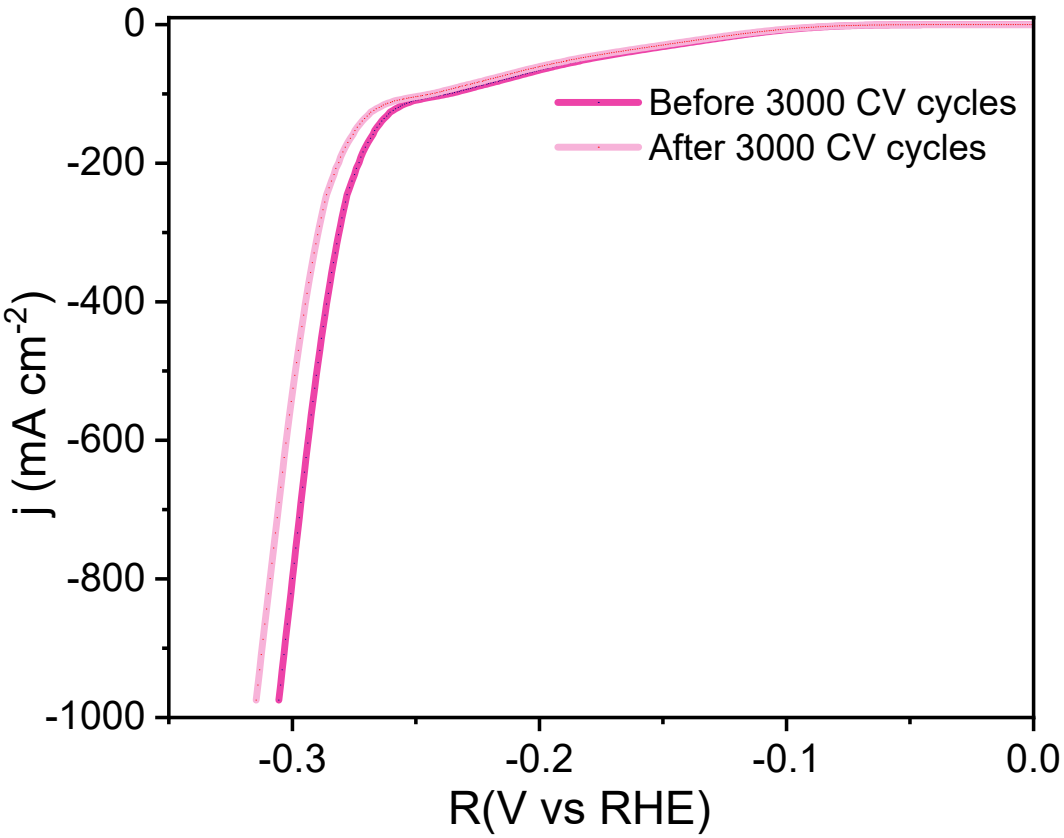


**S-16:** Chronoamperometric stability analysis of the PhosTriO7 catalyst toward the oxygen evolution reaction (OER) in 1.0 M KOH. The polarization curves recorded before and after 100 h of continuous operation display minimal deviation, demonstrating the excellent durability, structural robustness, and sustained electrocatalytic activity of PhosTriO7 under prolonged alkaline OER conditions.

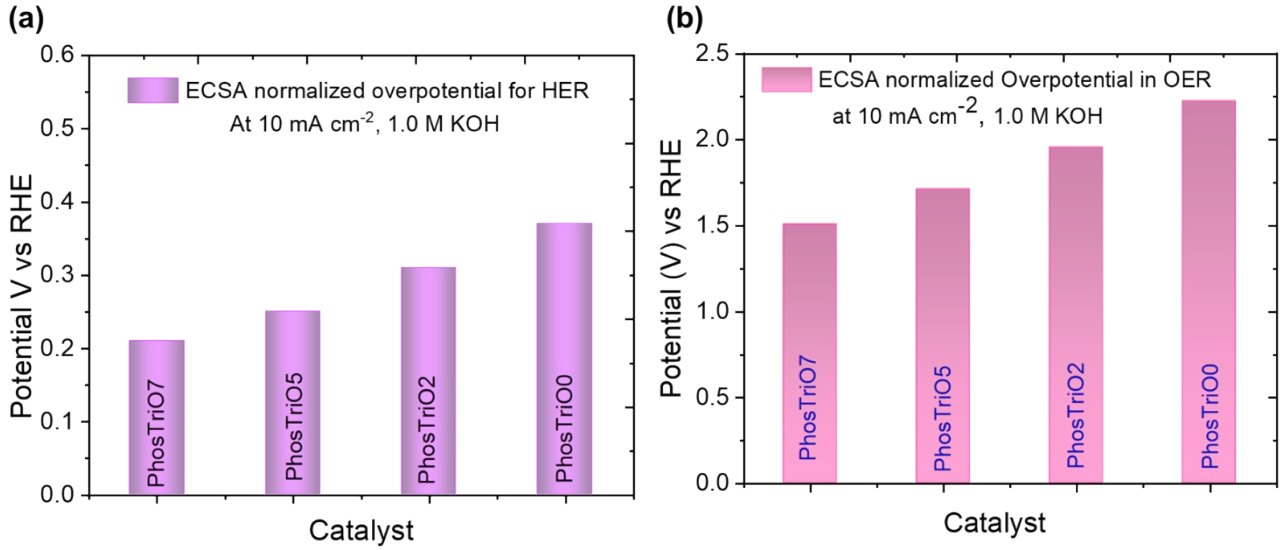


**S-17:** ECSA normalized overpotentials in case of HER and OER at 10 mA $cm^{-2}$ in 1.0 M KOH.

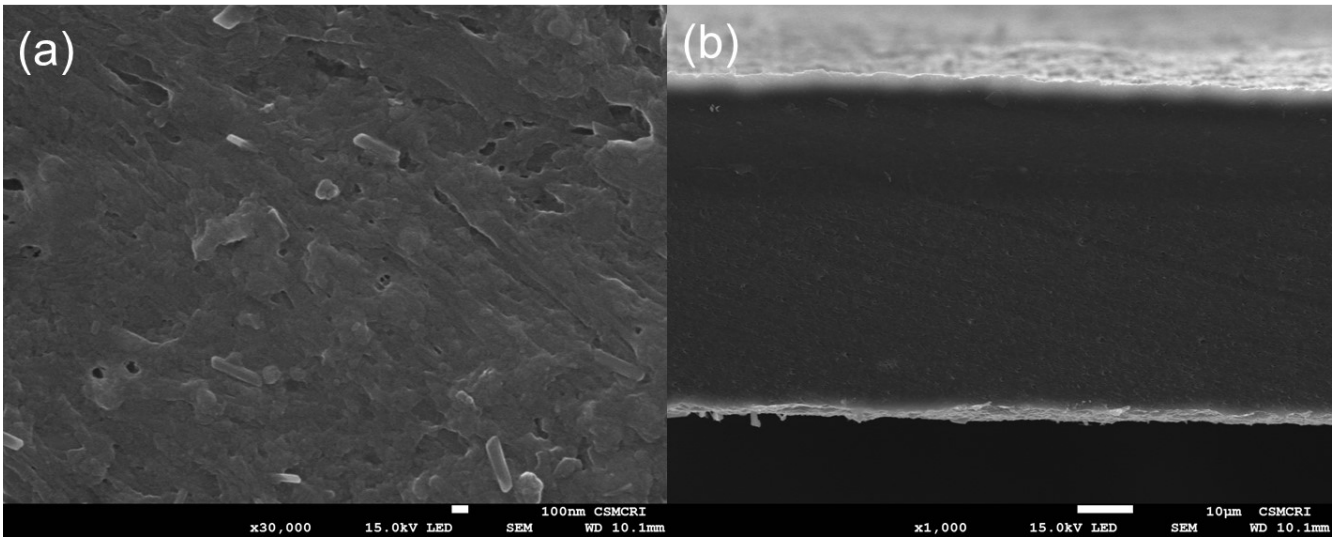


**S-18:** Post experiment SEM of the membrane.

**Table S1:** Atomic % of the different elements presented in the catalyst

| Elements | Atomic % |
|---|---|
| O (1s) | 37.99 |
| Mo (3d) | 12.98 |
| Ni (2p) | 28.96 |
| P (2p) | 9.36 |
| Ce (3d) | 10.71 |

**Table S2:** Physicochemical properties of the Styrion AEM after 250 hr stability test where: IEC (ion exchange capacity ($meqg^{-1}$), IC (Ionic conductivity, $mScm^{-1}$) and WU (water uptake (%))

| **Membrane** | **IEC** | **IC** | **WU** |
|---|---|---|---|
| **Styrion AEM** | **0.83** | **45** | **23** |